Unveiling the Post-PKS Redox Tailoring Steps in Biosynthesis of the Type II Polyketide Antitumor Antibiotic Xantholipin

Weike Zhang,[1] Lu Wang,[2] Lingxin Kong,[1] Tao Wang,[1] Yiwen Chu,[2] Zixin Deng,[1] and Delin You[1,*]

[1]State Key Laboratory of Microbial Metabolism and School of Life Sciences and Biotechnology, Shanghai Jiao Tong University, 1954 Huashan Road, Shanghai 200030, China

[2]Sichuan Industrial Institute of Antibiotics, Sichuan 610052, China

*Correspondence: dlyou@sjtu.edu.cn

DOI 10.1016/j.chembiol.2012.01.016

SUMMARY

Xantholipin from *Streptomyces flavogriseus* is a curved hexacyclic aromatic polyketide antitumor antibiotic. The entire 52 kb xantholipin (*xan*) biosynthetic gene cluster was sequenced, and bioinformatic analysis revealed open reading frames encoding type II polyketide synthases, regulators, and polyketide tailoring enzymes. Individual in-frame mutagenesis of five tailoring enzymes lead to the production of nine xantholipin analogs, revealing that the xanthone scaffold formation was catalyzed by the FAD binding monooxygenase XanO4, the δ-lactam formation by the asparagine synthetase homolog XanA, the methylenedioxy bridge generation by the P450 monooxygenase XanO2 and the hydroxylation of the carbon backbone by the FAD binding monooxygenase XanO5. These findings may also apply to other polycyclic xanthone antibiotics, and they form the basis for genetic engineering of the xantholipin and similar biosynthetic gene clusters for the generation of compounds with improved antitumor activities.

INTRODUCTION

Polycyclic xanthone antibiotics feature an angular fused hexacyclic skeleton with a xanthone structure (orange in Figure 1). They are active against fungal or Gram-positive bacteria, including methicillin-resistant *Staphylococcus aureus* and vancomycin-resistant *Enterococcus faecalis* (Peoples et al., 2008), or against several cancer cell lines (Kunimoto et al., 2003). Xantholipin (**1**) is a polycyclic xanthone antibiotic produced by *Streptomyces flavogriseus*. It possesses potent cytotoxicity against the leukemia cell line HL60 ($IC_{50} < 0.3$ μM) and the oral squamous carcinoma cell line KB ($IC_{50} < 2$ nM; Terui et al., 2002), and it was recently identified as a lead drug for the treatment of fibrotic diseases (Yuichi et al., 2003). The total chemical synthesis of another polycyclic xanthone antibiotic, FD-594, has been achieved, but it required many steps and did not produce sufficient amounts for medical testing (Masuo et al., 2009). Genetic engineering of the gene cluster may be suitable for this purpose.
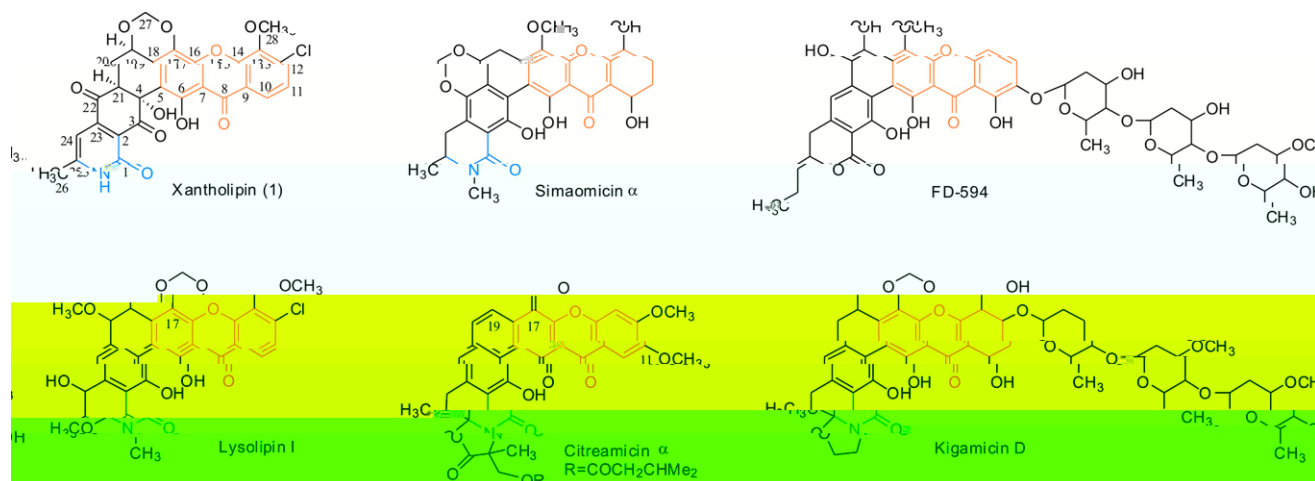
Biosynthetic studies and isotope-labeled precursor feeding experiments of polycyclic xanthone antibiotics, including simaomicin α

Figure 1. Structures of Xantholipin and Derivatives
Orange, xanthone; blue, cyclic amide.

insert size) using sib selection (McCormick, 1987). Sixteen overlapping fosmids were identified. To determine the relevance for the biosynthesis of **1**, a 40 kb DNA fragment was deleted from the *S. flavogriseus* genome by gene replacement using the remains of fosmid 28B8 after *Xho*I digestion and religation (Figure 2; Figure S1A available online). Two independently generated mutants no longer produced **1**, suggesting that the *xan* genes may have been deleted (Figure S1D). Fosmid 22E4, containing a central halogenase gene, was sequenced. It contained several putative antibiotic tailoring genes but, surprisingly, no PKS gene. Chromosome walking using PCR probes 2 and 3 (Figure 2, top) resulted in a minimal 92 kb contig flanked by fosmids 26G2 and 12A9. The 92,445 bp sequence contained 49 open reading frames (ORFs) that were likely to be involved in the biosynthesis of **1** (Figure 2 and Table 1). This was based on functional assignment (XanY1–Y5) and the presence of likely orthologs in the *llp* (lysolipin) and *pnx* (FD-594) gene clusters (Kudo et al., 2011; Lopez et al., 2010). Deletion of ORF1–5 or ORF6–9 from the *S. flavogriseus* genome produced normal looking colonies that still produced **1** (Figures 2 and S1), indicating that these ORFs were located outside the *xan* cluster.

Putative functions were assigned to most of the remaining 49 ORFs as shown in Figure 2 and Table 1. Six *xan* genes (black) encode three cyclases (C1–C3) and a type II minimal PKS consisting of the ketosynthase KS_α (XanF), chain length factor (CLF) KS_β (XanE), and acyl carrier protein (ACP; XanD). Five dispersed genes (green) were suspected for post-PKS tailoring: a halogenase (XanH) for the chlorination of C12, an asparagine synthetase homolog (XanA) for the formation of the amide ring, two *O*-methyltransferases (XanM1 and XanM2) for the methylation of the C13 and C17 hydroxyl groups, and an additional unassigned methyltransferase (XanM3). Consistent with the highly oxidized structure of **1**, 19 redox genes (pink and red) were identified. In addition to the biosynthetic machinery, five genes (*xanY1–Y5*, dark blue; not present in the *llp* and *pnx* gene clusters) are for the S-adenosyl methionine (SAM) recycling, and three genes (*xanB1–B3*, light blue; also without orthologs in the *llp* or *pnx* clusters) are for the synthesis of

malonyl-CoA extender units. There are also three putative regulatory and three resistance genes (yellow) and five ORFs without known functions (gray, *xanJ, xanP, xanG, xanL*, and *xanW*), also without orthologs in the *llp* or *pnx* clusters.

Biosynthesis of the δ-Lactam

Most polycyclic xanthones feature a cyclic amide, which is otherwise rare among aromatic polyketides (blue in Figure 1; FD-594 has a δ-lactone instead). In addition, there are various substituents on the amide nitrogen in the different polycyclic xanthones, such as a methyl group in lysolipin, an amino group in simaomicin, and more complicated heterocyclic structures in citreamicin α and Kigamicin D. The *xan* gene cluster contains an asparagine synthetase homolog, XanA, which strongly resembles the class II asparagine synthetase homolog LlpA (lysolipin) and the amide synthetase FdmV (Chen et al., 2010; fredericamycin A, not a xanthone), including the conserved active site and ligand binding site residues Arg50, Glu80, Asp103, Ser264, and Gly376 (Larsen et al., 1999). FdmV has been characterized to catalyze the formation of a hexacyclic amide, which is similar to the amide ring of **1**. XanA probably converts the polyketide-derived C1 carboxyl group to an amide, followed by the possibly spontaneous elimination of water to form ring F (Figure 3, conversion of compound **8a** to **9**).

To test this hypothesis in vivo, *xanA* was replaced by an apramycin resistance gene in the *S. flavogriseus* genome (Figure S1E). The Δ*xanA* mutant accumulated compound **8a** containing a chlorine and a xanthone structure but was devoid of nitrogen (Figures 3 and 4). From 14 l fermentation broth, 85 mg of compound **8a** was purified. ESI-Q-TOF MS, 1D and 2D nuclear magnetic resonance (NMR) spectra (^{1}H, ^{13}C, DEPT, HMBC, HSQC), provided the molecular formula $C_{26}H_{19}ClO_9$ and the structure (Figures 3, 4, S2, and S3). Different from our expectation, there was no spontaneous cyclization producing the α-pyrone derivative of **8a**; instead, a carboxyl group remained at C1, which was probably a more suitable substrate for XanA. The purified compound **8a** was then crystallized and X-ray diffraction was performed to further confirm the position

of chlorine at C12 of **8a**. The X-ray spectra clearly revealed the chlorine bound to C12; surprisingly, a lactone derivative **8b** was generated during the crystallization of **8a** from methanol (Figures 3 and S2).

Since *xanA* is within a group of 14 genes that might form an operon, inactivation of downstream genes by polar effects on transcription might have contributed to the phenotype of the *ΔxanA* mutant. Complementation expressing *xanA* from the high copy vector pJTU1278 partially (40%) restored production of **1** (Figure S1P), suggesting that deletion of *xanA*, and not inactivation of a downstream gene, was responsible for the production of **8a**. Therefore, XanA was required for the amidation of **8a**.

Bioinformatic Search for Genes for the Baeyer-Villiger Oxidation

We next addressed the biosynthesis of the xanthone ring, which is the characteristic feature of all polycyclic xanthone antibiotics and has not been elucidated genetically before. Studies on lysolipin I indicated that a Baeyer-Villiger oxidation was involved in the formation of xanthone (Bockholt et al., 1994), and epoxidation followed by a Baeyer-Villiger oxidation was proposed to be involved in the xanthone formation of the polycyclic xanthone antibiotic FD-594 (Kudo et al., 2011). Therefore, we selected four redox enzymes (O2, O4, O5, and T), which had orthologs in the FD-594 and lysolipin gene clusters, as possible candidates that might catalyze these reactions or, as we found out later, were involved in other steps for the biosynthesis of **1**.

XanO4 was between 29% and 31% identical to the atypical Baeyer-Villiger monooxygenases (BVMOs), including MtmOIV (mithramycin), JadH (jadomycin), and GilOI (gilvocarcin), all of which lack the typical sequence motif of type I BVMOs and are not related to the type II BVMOs (Beam et al., 2009; Gibson et al., 2005; Kharel et al., 2007; Rix et al., 2005). The similarities

contains a conserved NAD(P) binding site like XanO4, suggesting they use the same cofactor. XanT was proposed to be the partner protein supporting XanO4, but inactivation of *xanT* in *S. flavogriseus* did not cause accumulation of **6** (see below).

S. Flavogriseus Mutant Derivatives Lacking Redox Gene

The four genes *xanO2*, *xanO4*, *xanO5*, and *xanT* (Figure 2, underlined with black bars) had characteristics that suggest the likely involvement in xanthone formation. They were deleted separately in *S. flavogriseus* and replaced by an apramycin resistance cassette (Figure S1). LC-MS showed that each of the four mutants accumulated compounds that were different from **1** (Figure 4). Q-TOF MS was used to determine the molecular formulae of the main components in each extract (Figures 4 and S3).

The XanO4 blocked mutant accumulated large amounts of the red (483 nm) compound **6** (**1** was yellow). By optimizing the fermentation conditions and the isolation procedure, we obtained 48.5 mg of **6** from a 7 l culture of the ΔxanO4 strain. Evaluation of the ^1H, ^{13}C, DEPT, HMBC, HSQC NMR spectra (Figure S2 and Table S1) produced the structure of **6** (Figure 3). The NMR spectra resembled those of **8a**, but the signals for the ether bond of xanthone were missing, and a methoxylated anthraquinone was identified instead. (Note that C15 of **6** is replaced by O in **7**.)

The ΔxanO2, ΔxanO5, and ΔxanT mutants produced insufficient amounts of compounds for NMR analysis, and it was interesting to note that all of the three mutants accumulated more than one product, which implied that the primary reaction products were probably metabolized by other enzymes or underwent spontaneous reactions. XanT and XanO4 probably acted first, because the products from the deletion mutants did not contain chlorine or nitrogen. XanO2 and XanO5 probably performed late steps, because the accumulated products contained one chlorine and one nitrogen, like compound **1** (Figures 3 and 4). From the high-resolution molecular masses, the proposed functions of XanO2 and XanO5 in the biosynthetic pathway of **1** (see above), and the structures of **8a/8b** and **1,** compounds **11a** (accumulated by the ΔxanO2 mutant) and **15a** (accumulated by the ΔxanO5 mutant), probably had the structures shown in Figure 3. Structure **7** was proposed from the comparison of the known structures **6** and **8a/8b**, and **9** was proposed from the comparison between **8a/8b** and **1**. The proposed structures of the other compounds are explained below.

Introducing an integrative plasmid expressing *xanO2* from the *ermE** promoter (McDaniel et al., 1993) into the ΔxanO2 mutant only partially restored **1** production (Figure S1Q), possibly because the promoter was not suitable for XanO2 expression in *S. flavogriseus* or because the expression of the downstream *xan* genes was reduced.

XanO4 was purified from an *E. coli* clone. In the presence of XanO4, it oxidized NADPH to NADP and transferred the electrons to FAD. Compound **6**, the proposed substrate of XanO4, was not converted to compound **7** using NAD(P)H and FAD as cofactors (Figure S5). Therefore, XanO4 probably requires a partner protein to convert **6** to **7**. Unfortunately, XanT, the proposed partner protein of XanO4 (see above), could not be obtained in soluble form for enzymatic testing.

Bioactivity of Xantholipin and Putative Biosynthetic Intermediates

To determine how the oxidative modification during **1** biosynthesis affects bioactivity, we performed in vitro cytotoxicity assays of **6**, **8a**, **1**, and doxorubicin as a positive control. Table 2 shows that **1** was 10-fold more effective against a lung cancer cell line, 3-fold more effective against a colon cancer cell line, and equally effective against a leukemia than the commonly used anticancer drug doxorubicin. The precursors **6** and **8a** were, however, about 10^2- to 10^3-fold less potent. These data indicated that the post-PKS modifications were important for bioactivity.

Proposal for a Biosynthetic Pathway for 1

The proposed biosynthesis pathway of **1** (Figure 3) probably begins with the synthesis of malonyl-CoA from carboxylation of acetyl-CoA by the enzymes XanB1–B3 (probable acetyl-CoA carboxylase; Figure 2, light blue arrows; Table 1). These enzymes probably duplicate enzymes from the primary metabolism, which supply malonyl-CoA for fatty acid biosynthesis. Similar clusters occur in other antibiotic biosynthesis gene clusters, including that of pradimicin (Kim et al., 2007), but interestingly, there are no orthologs in the *llp* and *pnx* gene clusters.

Condensation of 13 malonate units by the minimal type II PKS (XanDEF; acyl carrier protein, ACP; chain length factor, CLF or KS_β; ketosynthase, KS_α) probably produces the hypothetical, enzyme-bound, and fully oxidized polyketide **2**. The three PKS subunits contained all the conserved active-site residues (Bisang et al., 1999). A phylogenetic analysis of KS_βs of type II PKSs showed that, as expected for the C26 polyketide chain of **1**, XanE clustered with the longer chain (C24–30) KS_βs (Figure S4A). Unusual for type II PKS gene clusters, including *llp* and *pnx*, *xanD* (ACP) was separate from the KS genes.

Three carbonyl reductions at C11, C17, and C19 were postulated to produce the hypothetical compound **3,** based on isotope-feeding experiments of lysolipin and citreamicin (Guy et al., 1991). They are probably performed by the 3-oxoacyl-ACP reductases XanZ3 and XanZ4, which have orthologs in the *llp* and *pnx* gene clusters (about 70% identity) and are similar to the characterized C19 ketoreductase (KR) BenL (benastatin; Lackner et al., 2007). C19 KRs are known exclusively from angucycline antibiotics, and usually there is only a single C19 KR in each cluster (Lackner et al., 2007). The *xan*, *llp*, *pnx*, and *grh* (griseorhodin) gene clusters encode two probable C19 KRs, which were different from most angucycline antibiotic gene clusters (Li and Piel, 2002). Since no C11 KR has been, to our best knowledge, reported before, a phylogenetic analysis of the C17 KRs and the C19 KRs was performed. It revealed that XanZ3 clustered with LlpZI, PnxG, GrhT, GrhO10, and known C19 KRs and XanZ4 clustered with LlpZIII and PnxW but not with known C17 KRs (Xu et al., 2005; Figure 5). XanZ3 was thus the likely C19 KR, and XanZ4, LlpZIII, and PnxW may belong to a new family of C11 KRs, which are exclusive to polycyclic xanthone antibiotics.

Guided by the C11 and C19 hydroxyl groups, the cyclases XanC1–C3 then form five C-C bonds (intramolecular aldol condensations) to form the angular 5-ring aromatic structure **4**. XanC1 resembled the first and second ring cyclase TcmN (tetracenomycin; McDaniel et al., 1995; Shen and Hutchinson, 1996).

Table 1. Deduced Functions of ORFs in the Xantholipin Biosynthetic Gene Cluster

Xan Proteins		Protein Homologs	
Gene (aa)	Proposed Function	Protein, Origin	Identity/Similarity (%)
xanY1 (472)	Adenosylhomocysteinase	SSDG_05037, S. pristinaespiralis	95/97
xanY2 (300)	Methylenetetrahydrofolate reductase	SSDG_05038, S. pristinaespiralis	84/89
xanY3 (1165)	Methionine synthase	SSCG_05781, S. clavuligerus	89/93
xanY4 (330)	Carbohydrate kinase	SsfX2, S. sp. SF2575	70/79
xanY5 (406)	SAM synthetase	SSCG_03814, S. clavuligerus	85/91
xanO1 (145)	Monooxygenase	SanK, S. sp. SANK 61196	33/51
xanS1 (407)	Dehydrogenase	LlpS, S. tendae	59/74
xanJ (242)	Unknown	ORF6, S. antibioticus	42/56
xanP (539)	Unknown	SBI_09782, S. bingchenggensis	69/78
xanG (391)	Unknown	LlpG, S. tendae	60/71
xanA (614)	δ-lactam formation	LlpA, S. tendae	72/80
xanR1 (227)	Transcriptional regulator	LlpRIII, S. tendae	49/61
xanO2 (400)	Cytochrome P450	LlpOIV, S. tendae	73/84
xanK (89)	3Fe-S ferredoxin	LlpK, S. tendae	67/77
xanU (709)	Antibiotic transporter	ORF27, S. globisporus	57/73
xanO3 (392)	FAD-binding monooxygenase	Krac_4468, Ktedonobacter racemifer	44/59
xanL (186)	Unknown	BSG1_19969, Bacillus sp. SG-1	33/52
xanH (471)	Halogenase	LlpH, S. tendae	70/85
xanQ (533)	Transporter	FdmT, S. griseus	46/60
xanM1 (339)	O-methyltransferase	LlpMIV, S. tendae	63/72
xanZ1 (285)	Reductase	LlpZII, S. tendae	59/73
xanN (431)	Antiporter	Veg3, uncultured soil bacterium	57/76
xanW (162)	Unknown	SACTE_4627, S. sp. SirexAA-E	48/67
xanR2 (153)	Transcriptional regulator	PnxR1, S. sp. TA-0256	34/53
xanM2 (340)	O-methyltransferase	LlpMIII, S. tendae	63/74
xanO4 (540)	FAD-binding monooxygenase	LlpOVIII, S. tendae	70/81
xanM3 (344)	O-methyltransferase	LlpMII, S. tendae	64/77
xanO5 (531)	FAD-binding monooxygenase	GrhO9, S. sp. JP95	43/58
xanS2 (228)	Dehydrogenase	LlpU, S. tendae	56/69
xanZ2 (302)	Oxidoreductases	SSAG_00456, S. sp. Mg1	80/87
xanR3 (335)	Transcriptional regulator	SACTE_0424, S. sp. SirexAA-E	83/87
xanB1 (447)	Biotin carboxylase	PdmP1, Actinomadura hibisca	63/74
xanB2 (174)	BCCP	PdmP2, Actinomadura hibisca	51/59
xanB3 (564)	Carboxyl transferase	ZhuF, S. sp. R1128	59/68
xanO6 (103)	Monooxygenase	LlpOII, S. tendae	59/68
xanO7 (115)	Monooxygenase	LlpOIII, S. tendae	58/71
xanZ3 (250)	3-oxoacyl-ACP reductase	LlpZI, S. tendae	70/83
xanO8 (153)	Monooxygenase	LlpB, S. tendae	65/77
xanC1 (155)	Cyclase	RubF, S. collinus	68/78
xanE (428)	Chain length factor	LlpE, S. tendae	68/77
xanF (425)	Ketosynthase	LlpF, S. tendae	80/89
xanC2 (144)	Cyclase	LlpCII, S. tendae	72/84
xanT (128)	CurD homolog	LlpT, S. tendae	71/84
xanO9 (472)	Oxidase	Aur2I, S. aureofaciens	47/62
xanO1 (148)	Monooxygenase	LlpQ, S. tendae	61/72
xanV (126)	CurD homolog	LlpV, S. tendae	72/84
xanZ4 (251)	3-oxoacyl-ACP reductase	LlpZIII, S. tendae	66/75
xanD (86)	ACP	SsfC, S.sp. SF2575	48/67
xanC3 (112)	Cyclase	LlpCIII, S. tendae	69/84

XanC1 may thus form the first two bonds at C9–C14 and C7–C16 in **1**. XanC3 was very similar to TcmI and JadI (jadomcyin), which have been proved to be responsible for "kinked ring" cyclization (Shen and Hutchinson, 1993), and may thus form the bond between C4 and C21 for ring E of compound **4**. XanC2 resembled several cyclases (RubD, GrhS, FdmD, and TcmJ), which may increase the yields of cyclized products by stabilizing the complex composed of the minimal PKS (Bao et al., 1998). There are no clues about which enzymes may perform the third and fifth cyclizations to form compound **4**.

Based on the proven structure of compound **6** (see below), the pentacyclic compound **4** needs to undergo three hydroxylation
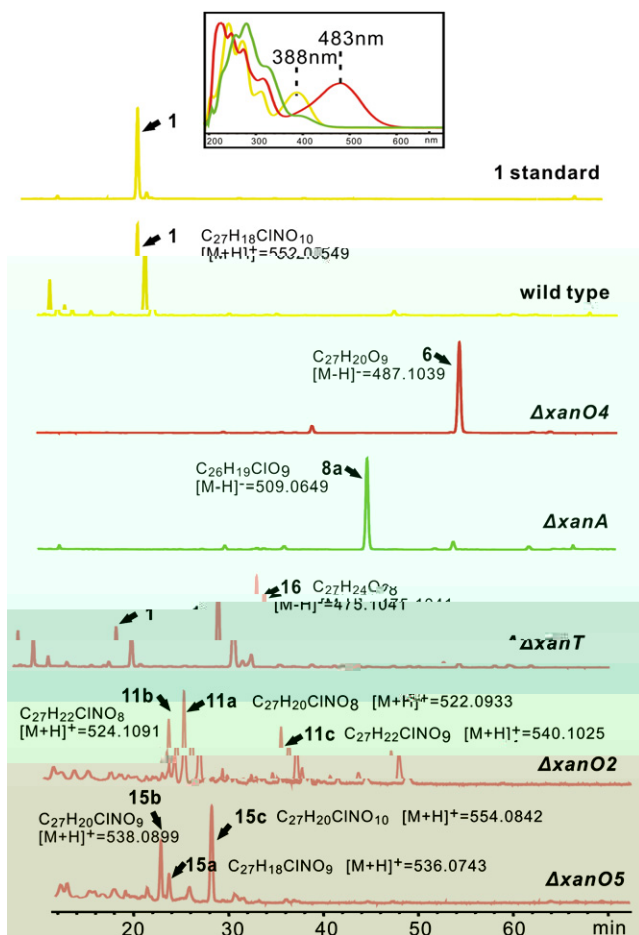
Figure 4. Analysis of Antibiotic Production by *S. Flavogriseus* and Its Mutant Derivatives

Top, UV spectra of compounds **1** (xantholipin, yellow), **6** (red), and **8a** (yellow). Bottom, HPLC traces (274 nm UV absorption). The formulas of the compounds were given by Q-TOF Mass shown in Figure S3. Note, **8b** was generated during the crystallization from methanol for X-ray analysis.

See also Figure S5.

steps at C6, C8, and C17, followed by oxidation to yield the anthraquinone structure of **5**, which was probably no longer attached to the ACP. Aromatic type II PKS gene clusters, including *xan*, do not contain a thioesterase, and it is not known how the molecules are released from the ACP (Staunton and Weissman, 2001).

Four small putative antibiotic biosynthesis monooxygenase (ABM) superfamily enzymes, XanO6, XanO7, XanO8, and XanO10, were predicted to be associated with the hydroxylations of the aromatic backbone. XanO8 was similar to FdmM (48% identity), which has been characterized to hydroxylate C6 nearest to the inside bend of fredericamycin (Chen et al., 2009), which corresponds to position C6 in **5**. Therefore, XanO8 probably hydroxylates C6. XanO6 and XanO7 were similar to PdmH, which has been proved to be responsible for quinone formation in the pentangular polyphenol backbone of pradimicin (Zhan et al., 2008). XanO10 was similar to FdmM1 (48% identity) hydroxylating C8 in fredericamycin (Chen et al.,

2009). The two reactions both correspond to the oxidation at C8 in **5**. XanO6, XanO7, and XanO10 were thus candidates for the hydroxylation at C8 in **4**. The oxidation of **4** at C17 may also be performed by one of the three enzymes.

An additional gene, *xanT* (SchA/CurD superfamily), also encodes a small protein similar to ABM monooxygenase and has homologs in the *llp* and *pnx* clusters. XanT was the possible enzyme that supports XanO4 in the formation of the xanthone structure. Inactivation of *xanT* resulted in the accumulation of a new metabolite **16** but did not abolish **1** production (Figure 4). Q-TOF analysis revealed that **6** and **16** contained the same number of carbons but **16** lacked an oxygen (Figure S3), suggesting that XanT acted on a less oxidized precursor of **6** before the xanthone was synthesized. The residual production of **1** in these mutants might have resulted from nonspecific activities from unidentified endogenous enzymes.

One of the three putative S-adenosyl-L-methionine-dependent methyltransferases (SAM-MTases; XanM1, 2, or 3) then transfers a methyl group to the C17 hydroxyl group of **5** to produce **6**, which was accumulated by the *ΔxanO4* mutant (see above). The hypothetical compound **10** contains two methoxy groups. XanM1 and XanM2 resembled *O*-methyltransferases, and XanM3 contains motifs for *O*- and *C*-methyltransferases. XanM1 and XanM2 were thus likely to be involved in the methylation of the C13 and C17 hydroxyl groups. The fully characterized compounds **6** and **8a** were *O*-methylated at C17 but not at C13. The C13 *O*-methylation may thus be specific for the hypothetical compound **9**, which contains the chlorinated xanthone and the δ-lactam.

XanY1–Y5, encoded by successive genes on the left side of the *xan* cluster, are a complete set of enzymes for the recycling of S-adenosylhomocysteine (a by-product in the SAM-dependent methylation reaction) to SAM (Haagen et al., 2006). These five genes are presumably required to ensure the supply of sufficient SAM precursor for the two methylations during the late growth phase, as has been proposed for saframycin biosynthesis (Li et al., 2008). Inactivation of XanY3-Y5 decreased the production of **1** about two-fold, which might have been caused by the insufficient supply of the methyl group from SAM (Figure S1). The residual **1** production probably utilized SAM from the primary biosynthetic pathway.

XanO4, probably together with an unidentified protein, catalyzes xanthone formation resulting in **7** because deletion of XanO4 resulted in the accumulation of **6** (see above). GrhO1 and GrhO5 (similar to XanO4) act together to catalyze three carbon-carbon bond cleavages for the biosynthesis of the
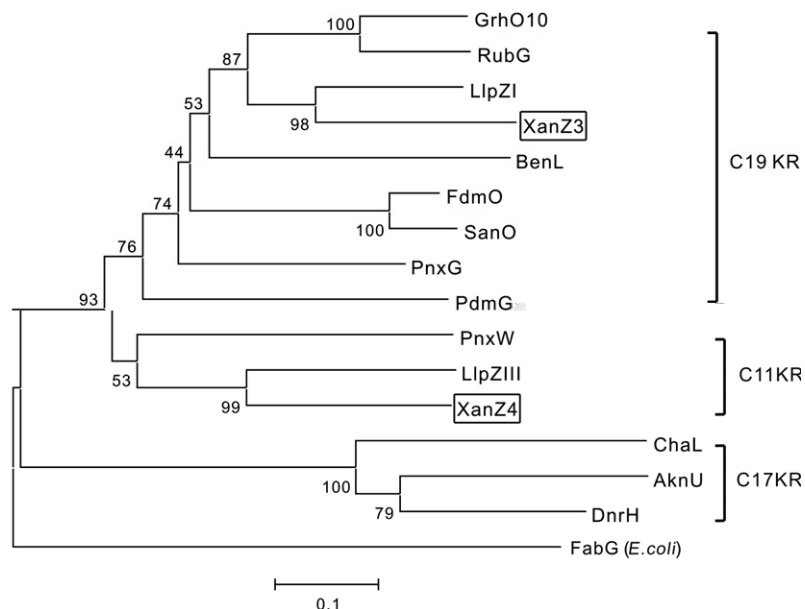
Figure 5. Phylogenetic Analysis of the XanZ3, XanZ4, and Their Homologs
PDB ID codes: LlpZI, CAM34340; GrhO10, AAM33668; RubG, AAG03071; BenL, CAM58804; FdmO, AAQ08926; SanO, ADG86325; PnxG, BAJ52686; LlpZIII, CAM34370; PnxW, BAJ52708; ChaL, CAH10174; AknU, AF264025; DnrH, AAA65202; FabG, EGT67884.
See also Figure S4.

spiroketal polyketide griseorhodin (Yunt et al., 2009). A two enzyme mechanism, including the XanO4 homolog PnxO4, was proposed for the xanthone ring formation for FD-594 (Kudo et al., 2011). Biosynthesis of the other polycyclic xanthone antibiotic lysolipin may thus also implicate a two component system, including the XanO4 homolog LlpOVIII to form the xanthone structure.

The mechanism of xanthone formation remains uncertain. XanO4 may cleave the C14-C15 or the C15-C16 bond. We proposed two alternative paths for the formation of the xanthone scaffold from **6** (Figure S6). The two paths share a Baeyer-Villiger oxidation catalyzed by XanO4, converting the quinone of **6** to a lactone via a "Criegee" intermediate. After that, the lactone may undergo a second round of Baeyer-Villiger oxidation, and the resultant circular carbonate ester is formed, followed by a decarboxylation reaction to produce **7** (path A). Alternatively, the lactone is hydrolyzed and recyclized via an intramolecular OH-attack. The resultant intermediate is hydroxylated at C7 followed by a decarboxylation and dehydration to yield **7** (path B). In both cases some additional, unidentified protein or cofactor may be required for the reaction.

Chlorination of **7** at C12 by XanH produces **8a**, which was fully characterized. XanH, the only putative halogenase of the *xan* gene cluster was 70% identical to LlpH (lysolipin biosynthesis), which is a nonheme, flavin-dependent halogenase (Lopez et al., 2010). Enzymes in this class catalyze the formation of carbon-halogen bonds at electron-rich positions, using $FADH_2$, a halide ion (usually Cl^-), and molecular oxygen (Yeh et al., 2007). The reduced flavin is provided by a partner flavin reductase, which could not be located within the sequenced 92 kb region. XanH seemed to be specific for **7** containing the xanthone structure, because it did not chlorinate **6** in the *ΔxanO4* mutant.

The next step is the δ-lactam (ring F) formation by the amide synthetase XanA (resembled asparagine synthetase; see above). Inactivation of XanA accumulated an expected carboxylic acid

8a and the trans-complementation restored **1** biosynthesis. This indicated that XanA was most probably required for the incorporation of the nitrogen and the formation of the characteristic δ-lactam ring to produce **9**. Compound **6**, that accumulated in the *ΔxanO4* mutant, was not amidated by XanA, suggesting that the xanthone structure, the chlorine or both may be important for XanA activity (Figure 3). This was in line with FdmV (fredericamycin), which can utilize a wide range of nitrogen sources but is specific for the fredericamycin precursor (Chen et al., 2010). Multiple alignments of FdmV homologs revealed that the Cys2, which is indispensable for glutaminase activity, was mutated to Ser in PdmN (pradimicin) and GrhP (griseorhodin), implying that their ability to hydrolyze Gln was lost (Chen et al., 2010). In the case of PdmN, L-Ala was still used as a nitrogen source instead of free NH_3 (Kim et al., 2007). The putative amide synthetases for citreamicin and kigamicin D feature the C2S mutation and may utilize unusual amino acids to form the heterocyclic structures.

C13 *O*-methylation by XanM1 or XanM2 produces **10**, which is then hydroxylated at C19 to produce **11a**. The identity of the oxidase for the C19 hydroxylation of **10** remains uncertain.

Bioinformatic analysis and the gene replacement experiment (see above) suggested that XanO2, the only P450 monooxygenase in the *xan* gene cluster, may convert **11a** to **12** (methylenedioxy bridge formation). Small amounts of a compound with the same formula as **11a** (calculated 522.0950, observed 522.0933, resulting in the same formula) was isolated from the *ΔxanO2* mutant. Two other compounds, **11b** and **11c,** with a UV absorption similar to compound **8a** (380nm), were probably shunt products derived from **11a** with added H_2 or H_2O, respectively. Their structures were not characterized by NMR because of insufficient yield. Compound **11a** was a suitable substrate for methylenedioxy bridge formation. Considering all the information above, XanO2 probably catalyzed a reaction between the C19 hydroxyl group and the C17 methoxy group to form the methylenedioxy bridge of **12**.

Biochemical logic suggested that four steps are needed to convert **12** to **1**; hydroxylation of **12** at C22, followed by formation of the quinone ring E and reduction of the C4-C21 double bond results in **15a**, which was the predicted substrate for C4 hydroxylation.

Hydroxylation at C22 of **12** is similar to the three earlier hydroxylations at C6, C8, and C17 of **4** and was proposed to come after the methylenedioxy bridge formation by XanO2. Analysis mentioned above assigned four possible candidate enzymes for the three hydroxylations. One of the four putative

monooxygenases, XanO6, 7, 8, or 10, may perform this step. No enzyme has been identified for the formation of quinone in ring E.

Prior to the C4 hydroxylation, the double bond between C4 and C21 has to be reduced. Two reductases, other than the 3-oxoacyl-ACP reductase, XanZ1 and XanZ2, are encoded in the *xan* cluster. XanZ1 is homologous to a F420-dependend reductase and XanZ2 belongs to the aldo/keto reductase superfamily, who use soluble NAD(P)H as electron donor. It is still uncertain which one of the two reductases is responsible for the reduction of the C4-C21 double bond in the conversion of **14** to **15a**.

Compound **15a,** accumulated by the *ΔxanO5* (polyketide hydroxylase) mutant, possibly has the expected substrate structure for C4 hydroxylation. Compounds **15b** and **15c** were likely shunt products derived from **15a**, with added H_2 or H_2O. Thus, XanO5, was most probably responsible for the C4 hydroxylation of **15a** to complete the biosynthesis of **1**.

SIGNIFICANCE

Xantholipin is a polycyclic xanthone antibiotic representing a class of molecules exhibiting antitumor, antibacterial, and antifungal bioactivity. The biosynthetic pathways for these compounds are of great interest, as they undergo uncommon prearomatic modifications and reveal unusual functional groups. We have identified the biosynthetic gene cluster and its boundaries, which features an unusual C11 ketoreductase for the pre-aromatic reduction of the tridecaketide backbone of xantholipin. We also obtained nine compounds accumulated by blocked pathway mutants, two of which were fully characterized. This gave insight into the biosynthesis of three main structural features of xantholipin, including a FAD binding monooxygenase for the xanthone scaffold, an amide synthetase for the amide bond formation, and, to our knowledge, the first identification of a bacterial P450 monooxygenase for methylenedioxy bridge formation. Characterization of the biosynthetic pathway of xantholipin provides the opportunity to understand unusual modifications involved in the biosynthesis of polycyclic xanthone antibiotics and generate libraries of derivative compounds for structure-activity relationship studies by genetic engineering.

EXPERIMENTAL PROCEDURES

Bacteria Strains, Plasmids, Primers, Culture Conditions, and General Techniques

Bacterial strains and plasmids are listed in Table S1, primers are in Table S2. *Escherichia coli* DH10B, BW25113, and ET12567/pUZ8002 were used for cloning, λ-Red-mediated recombination or, conjugation between *E. coli* and *Streptomyces spp.,* respectively (Gust et al., 2003; Paget et al., 1999). *S. flavogriseus* SS101 was the wild-type xantholipin producer used for the generation of mutant strains. ISP-3 solid medium was used for *S. flavogriseus* sporulation and SFM solid medium (Kieser et al., 2000) for conjugation between *E. coli* and *Streptomyces*. Liquid seed medium (per liter: 10 g glucose, 25 g soluble starch, 2 g yeast extract, 5 g fish meal, 3 g pharmamedia, 3 g casein, and 2 g calcium carbonate [pH 7.2]) was used for growing mycelia for the isolation of total DNA and liquid fermentation medium (per liter: 20 g oatmeal, 10 g pharmamedia, 5 g fish meal, 10 g glucose, 25 g dextrin, 2 g yeast extract, and 3 g calcium carbonate [pH 7.2]) was used for xantholipin

production. For *Streptomyces*, thiostrepton and apramycin were used at 12.5 μg/ml and 15 μg/ml in solid and liquid media, respectively.

The unstable *Streptomyces* plasmids pHZ1358 (Sun et al., 2009) and its derivative plasmid pJTU1278 were used for gene inactivation. pMD18-T (TaKaRa, Dalian, China) and pBlueScript II SK(+) (Stratagene, La Jolla, CA, USA) were used for DNA sequencing, and pRSET B (Invitrogen, Shanghai, China) was used for heterologous protein expression. Recombinant DNA techniques for *E. coli* and *Streptomyces* were as described (Kieser et al., 2000; Sambrook and Russell, 2000).

S. Flavogriseus Fosmid Library

A library of *S. flavogriseus* DNA in *E.coli* EPI300-T1[R] was constructed in the vector pCC1FOS using CopyControl Fosmid Library Production Kit (Epicenter, Madison, WI, USA). Conserved motifs of nonheme halogenases involved in the biosynthesis of lysolipin were identified by sequence alignment and used to design the PCR primers probe1-F/R. The fosmid library was screened by PCR and fosmid 22E4 was isolated. Two more primer pairs, (probe2-F/R, probe3-F/R) were used to isolate fosmids 26G2 and 12A9, which cover the entire xantholipin biosynthesis gene cluster (Figure 2).

Replacement in *S. Flavogriseus*

To genetically inactivate the putative xantholipin gene cluster, fosmid 28B8 was completely digested by *Xho*I and religated to give pJTU3923, which lacks 40 kb from *xanU* to *orf9* (Figure 2, open box). Then a 3.0 kb BamHI fragment from pJTU3923, containing the remains of 28B8, was cloned into the BamHI site of pBlueScriptII SK(+) to give pJTU3852. A 1.4 kb fragment containing *aac(3)IV* was amplified from pHGF9827 using primers ZWK1-F/R and inserted into the unique *Xho*I site of pJTU3852 to produce pJTU3851. Subsequently, the 4.4 kb BamHI fragment from pJTU3851 was inserted into the BamHI site of the unstable *Streptomyces* vector pJTU1278 to give the 40 kb fragment deletion vector pJTU3853, which was then introduced into *S. flavogriseus* by conjugation to generate mutant ZWK1 by double crossover (Figure S1A). PCR using primers ZWK1-DF/DR confirmed the deletion (not shown). The determination of the boundaries of the *xan* cluster and construction of individual gene inactivation mutants is described in detail in Figure S1 and the Supplemental Experimental Procedures.

Analysis of Xantholipin Metabolites

S. flavogriseus was grown for six days in fermentation medium at 30°C, collected by centrifugation and extracted overnight with n-butanol. The supernatant was collected by centrifugation, dried under reduced pressure and dissolved in methanol. The methanol extract was analyzed by LC-MS (Agilent 1100 series LC/MSD Trap system, Agilent, Santa Clara, CA, USA). The HPLC was operated at a flow rate of 0.5 ml/min on a Waters SB-C18 (3.9 × 150 mm, 2 μm) column. Solvent A was 0.2% formic acid and 0.1% TFA, solvent B was acetonitrile. The program used a gradient from 20 to 55% solvent B over 50 min. The elution was monitored at 274 nm and analyzed using the Waters Millennium Chromatography Manager (Agilent). The ion trap mass spectrometer was operated in the positive ion mode. Drying gas flow was 8 l/min, and nebulizer pressure was 206.8 kPa. Drying gas temperature was 325°C, and the fragmentation was between 1.0 V to 1.8 V. An Agilent 6530 Accurate-Mass Q-TOF LC/MS was used for high-resolution mass measurements.

Production, Isolation, and Characterization of Compound 6 and 8a/b

Compounds **6** and **8a** were produced, isolated, and analyzed using method similar to each other. First, the two mutant strains *S. flavogriseus* ZWK8 and ZWK2 were grown at 30°C in 7 l and 14 l of fermentation medium, respectively; each 10 l fermenter contained 7 l culture. After six days, the mycelia were harvested by centrifugation and the compounds were extracted from the mycelium by 7 l and 10 l of methanol, respectively. The extract was then evaporated to 2 l, and the remaining liquid was re-extracted by 2 l of ethyl ethanoate. Then the organic phase was concentrated and fractionated by silica gel column chromatography (chloroform/methanol, gradient elution). Fractions containing the target compound were combined, dried, and further purified by preparative LC (C18 column, 40%–60% methanol in H_2O over 10 min for **6**, 50%–80% methanol in H_2O over 10 min for **8a**). Final purification was accomplished by preparative HPLC (C18 column, gradient for **6**; 30 to

60% acetonitrile, [pH 3.5] H_2O with acetic acid over 10 min; gradient for **8a**, 30% to 80% acetonitrile, [pH 3.5] H_2O with acetic acid over 15 min). We obtained 48.5 mg of **6** and 84.5 mg of **8a**.

The structures of **6** and **8a** were characterized using ^1H, ^{13}C NMR, DEPT, HSQC, HMBC (Table S1). Single crystals of **8b** were prepared by recrystallization in methanol, and the X-ray analysis was accomplished at the Shanghai Institute of Organic Chemistry.

Expression, Purification, and Analysis of the BVMO XanO4

For the heterologous expression of XanO4 in *E. coli* BL21(DE3)/pLysE/pJTU3889 (pRSET B containing *xanO4),* a BamHI-EcoRI fragment was amplified from genomic DNA using primers XanO4-F/R (Tables S2 and S3). The transformants were grown in 1 l of LBBS (per liter: 10 g trptone, 5 g yeast extract, 10 g sodium chloride, 185.9 g D-sorbitol, and 0.31 g betaine) medium containing ampicillin and chloramphenicol at 37°C to A_{600} 0.6 before addition of isopropy-β-D-thiogalactoside (IPTG) to 0.2 mM, followed by incubation at 18°C for 24 hr. His_6-XanO4 was absorbed to a 1 ml HisTrap HP column (GE Healthcare) and eluted at 1 ml/min^{-1} by a gradient of imidazole from 5 mM to 500 mM over 30 min in 150 mM NaCl and 20 mM Tris-HCl (pH 7.9) using the Amersham Biosciences ÄKTA FPLC.

XanO4-catalyzed oxidation of NADPH was monitored at 30°C at 340 nm, in 50 mM PBS (pH 7.5), containing 0.5 mM NADPH, 0.2 mM FAD, 40 μM XanO4, and 80 μM **6**.

Bioactivity Assay

Cell proliferation was determined using the methyl thiazolyl tetrazolium (MTT) assay for A-594, HCT-116, and P388 cells. Two thousand cells in 100 μl media per well were placed in a 96-well plate and allowed to incubate overnight at 37°C. Then, six different concentrations of xantholipin, **6**, or **8a** in DMSO were added to the cells in triplicate. After 72 hr, 20 μl 5 mg ml^{-1} MTT was added. After 3 hr, the supernatant was removed and 100 μl DMSO was added to each well. Cell proliferation was assayed colorimetrically using a SpectraMAX340 comparing 550 nm and 690 nm absorptions. All cells were cultured according to ATCC or DSMZ guidelines. Prism (GraphPad) was used for analysis.

Phylogenetic Analysis

Multiple sequences were aligned using ClustalW (Thompson et al., 1994), and the phylogenetic trees were generated by MEGA (version 3.1; Kumar et al., 2004) using neighbor-joining with Poisson correction and 1,000 replicate bootstrap analysis. The sequence of *E. coli* FabG was used as an outgroup to root the tree in Figure 5. To validate the tree topology, minimum evolution was also used as a distance method. Both methods gave similar tree topologies.

ACCESSION NUMBERS

The complete DNA and deduced protein sequences of the *xan* gene cluster reported in this paper have been deposited in GenBank under the accession number GQ421798.

SUPPLEMENTAL INFORMATION

Supplemental Information includes six figures, three tables, and Supplemental Experimental Procedures and can be found with this article online at doi:10.1016/j.chembiol.2012.01.016.

REFERENCES

Bao, W., Wendt-Pienkowski, E., and Hutchinson, C.R. (1998). Reconstitution of the iterative type II polyketide synthase for tetracenomycin F2 biosynthesis. Biochemistry *37*, 8132–8138.

Beam, M.P., Bosserman, M.A., Noinaj, N., Wehenkel, M., and Rohr, J. (2009). Crystal structure of Baeyer-Villiger monooxygenase MtmOIV, the key enzyme of the mithramycin biosynthetic pathway. Biochemistry *48*, 4476–4487.

Bisang, C., Long, P.F., Cortés, J., Westcott, J., Crosby, J., Matharu, A.L., Cox, R.J., Simpson, T.J., Staunton, J., and Leadlay, P.F. (1999). A chain initiation factor common to both modular and aromatic polyketide synthases. Nature *401*, 502–505.

Bockholt, H., Udvarnoki, G., Rohr, J., Mocek, U., Beale, J.M., and Floss, H.G. (1994). Biosynthetic-studies on the xanthone - antibiotics lysolipin-X and lysolipin-I. J. Org. Chem. *59*, 2064–2069.

Carter, G.T., Goodman, J.J., Torrey, M.J., Borders, D.B., and Gould, S.J. (1989). Biosynthetic origin of the carbon skeleton of simaomicin α, a hexacyclic xanthone antibiotic. J. Org. Chem. *54*, 4321–4323.

Chen, Y., Wendt-Pienkoski, E., Rajski, S.R., and Shen, B. (2009). *In vivo* investigation of the roles of FdmM and FdmM1 in fredericamycin biosynthesis unveiling a new family of oxygenases. J. Biol. Chem. *284*, 24735–24743.

Chen, Y.H., Wendt-Pienkowski, E., Ju, J.H., Lin, S.J., Rajski, S.R., and Shen, B. (2010). Characterization of FdmV as an amide synthetase for fredericamycin A biosynthesis in *Streptomyces griseus* ATCC 43944. J. Biol. Chem. *285*, 38853–38860.

Decker, H., Motamedi, H., and Hutchinson, C.R. (1993). Nucleotide sequences and heterologous expression of tcmG and tcmP, biosynthetic genes for tetracenomycin C in *Streptomyces glaucescens*. J. Bacteriol. *175*, 3876–3886.

Gibson, M., Nur-e-alam, M., Lipata, F., Oliveira, M.A., and Rohr, J. (2005). Characterization of kinetics and products of the Baeyer-Villiger oxygenase MtmOIV, the key enzyme of the biosynthetic pathway toward the natural product anticancer drug mithramycin from *Streptomyces argillaceus*. J. Am. Chem. Soc. *127*, 17594–17595.

Guengerich, F.P. (2003). Cytochrome P450 oxidations in the generation of reactive electrophiles: epoxidation and related reactions. Arch. Biochem. Biophys. *409*, 59–71.

Gust, B., Challis, G.L., Fowler, K., Kieser, T., and Chater, K.F. (2003). PCR-targeted *Streptomyces* gene replacement identifies a protein domain needed for biosynthesis of the sesquiterpene soil odor geosmin. Proc. Natl. Acad. Sci. USA *100*, 1541–1546.

Guy, T.C., Donald, B.B., Joseph, J.G., Joseph, A., Michael, G., William, M.M., and Cedric, J.P. (1991). Biosynthetic origins of the polycyclic xanthone antibiotic, citreamicin. J. Chem. Soc., Perkin Trans. *1*, 2215–2219.

Haagen, Y., Glück, K., Fay, K., Kammerer, B., Gust, B., and Heide, L. (2006). A gene cluster for prenylated naphthoquinone and prenylated phenazine biosynthesis in *Streptomyces cinnamonensis* DSM 1042. Chem. Bio. Chem. *7*, 2016–2027.

Ikezawa, N., Iwasa, K., and Sato, F. (2007). Molecular cloning and characterization of methylenedioxy bridge-forming enzymes involved in stylopine biosynthesis in *Eschscholzia californica*. FEBS J. *274*, 1019–1035.

Kharel, M.K., Zhu, L., Liu, T., and Rohr, J. (2007). Multi-oxygenase complexes of the gilvocarcin and jadomycin biosyntheses. J. Am. Chem. Soc. *129*, 3780–3781.

Kieser, T., Bibb, M.J., Buttner, M.J., Chater, K.F., and Hopwood, D.A. (2000). Practical *Streptomyces* Genetics (Norwich, UK: John Innes Fundation).

Kim, B.C., Lee, J.M., Ahn, J.S., and Kim, B.S. (2007). Cloning, sequencing, and characterization of the pradimicin biosynthetic gene cluster of *Actinomadura hibisca* P157-2. J. Microbiol. Biotechnol. *17*, 830–839.

Kondo, K., Eguchi, T., Kakinuma, K., Mizoue, K., and Qiao, Y.F. (1998). Structure and biosynthesis of FD-594; a new antitumor antibiotic. J. Antibiot. *51*, 288–295.

Kudo, F., Yonezawa, T., Komatsubara, A., Mizoue, K., and Eguchi, T. (2011). Cloning of the biosynthetic gene cluster for naphthoxanthene antibiotic FD-594 from *Streptomyces* sp. TA-0256. J. Antibiot. *64*, 123–132.

Kumar, S., Tamura, K., and Nei, M. (2004). MEGA3: Integrated software for Molecular Evolutionary Genetics Analysis and sequence alignment. Brief. Bioinform. *5*, 150–163.

Kunimoto, S., Someno, T., Yamazaki, Y., Lu, J., Esumi, H., and Naganawa, H. (2003). Kigamicins, novel antitumor antibiotics. II. Structure determination. J. Antibiot. *56*, 1012–1017.

Lackner, G., Schenk, A., Xu, Z., Reinhardt, K., Yunt, Z.S., Piel, J., and Hertweck, C. (2007). Biosynthesis of pentangular polyphenols: deductions from the benastatin and griseorhodin pathways. J. Am. Chem. Soc. *129*, 9306–9312.

Larsen, T.M., Boehlein, S.K., Schuster, S.M., Richards, N.G., Thoden, J.B., Holden, H.M., and Rayment, I. (1999). Three-dimensional structure of *Escherichia coli* asparagine synthetase B: a short journey from substrate to product. Biochemistry *38*, 16146–16157.

Li, A., and Piel, J. (2002). A gene cluster from a marine *Streptomyces* encoding the biosynthesis of the aromatic spiroketal polyketide griseorhodin A. Chem. Biol. *9*, 1017–1026.

Li, L., Deng, W., Song, J., Ding, W., Zhao, Q.F., Peng, C., Song, W.W., Tang, G.L., and Liu, W. (2008). Characterization of the saframycin A gene cluster from *Streptomyces lavendulae* NRRL 11002 revealing a nonribosomal peptide synthetase system for assembling the unusual tetrapeptidyl skeleton in an iterative manner. J. Bacteriol. *190*, 251–263.

Lopez, P., Hornung, A., Welzel, K., Unsin, C., Wohlleben, W., Weber, T., and Pelzer, S. (2010). Isolation of the lysolipin gene cluster of *Streptomyces tendae* Tü 4042. Gene *461*, 5–14.

Masuo, R., Ohmori, K., Hintermann, L., Yoshida, S., and Suzuki, K. (2009). First stereoselective total synthesis of FD-594 aglycon. Angew. Chem. Int. Ed. Engl. *48*, 3462–3465.

McCormick, M. (1987). Sib selection. Methods Enzymol. *151*, 445–449.

McDaniel, R., Ebert-Khosla, S., Hopwood, D.A., and Khosla, C. (1993). Engineered biosynthesis of novel polyketides. Science *262*, 1546–1550.

McDaniel, R., Ebert-Khosla, S., Hopwood, D.A., and Khosla, C. (1995). Rational design of aromatic polyketide natural products by recombinant assembly of enzymatic subunits. Nature *375*, 549–554.